Jour. Geol. Soc. India (2022) 98:479-486
https://doi.org/10.1007/s12594-022-2005-2

ORIGINAL ARTICLE

Mapping of Reservoir Properties using Model-based Seismic Inversion and Neural Network Architecture in Raniganj Basin, India

Abir Banerjee[1,*] and Rima Chatterjee[2]

[1]Department of Well Logging, Oil and Natural Gas Corporation Limited, Bokaro - 827 001, India
[2]Department of Applied Geophysics, Indian Institute of Technology (ISM), Dhanbad - 826 004, India
E-mail: *Banerjee_Abir@ongc.co.in*; rima_c_99@yahoo.com*

Received: 14 July 2021/ Revised form Accepted: 3 September 2021

ABSTRACT

Reservoir characterization is necessary to compute reservoir parameters for hydrocarbon potential and production optimization. The limitation of robust data and the presence of cultural noise is a constraint for reservoir characterization in the Raniganj basin located in India. Based on available well logs and two-dimensional post-stack seismic data, a model-based seismic inversion is executed to generate acoustic impedance by converting acoustic reflectivity into rock elastic parameters. Moreover, the seismic attributes obtained from the inversion are implemented in neural network architectures to map shale volume, Young's modulus, and Poisson's ratio. Error analysis between predicted and actual results demonstrate multi-layered feed-forward or probabilistic neural network display a better result in obtaining reservoir parameters. The mapped reservoir section shows the acoustic impedance varying from 5000 to 16,000 (g/cc)*(m/s), shale volume ranging from 15% to 55%, Young's modulus, and Poisson's ratio vary from 0.5-9.5 GPa and 0.23-0.27 respectively. Cross-plot between Young's modulus versus Poisson's ratio classifies lithology from brittleness and it increases with depth. Neural network architectures help to identify the best model in delineating shale barriers for designing hydraulic fracturing treatments. Results from this study have added significant values in engineering application and will help in ongoing coalbed methane exploration and future geomechanical studies. However, limitations exist in resolving thin coal seams as the seismic resolution depends on the wavelength, velocity, and frequency of waves in the formation.

INTRODUCTION

The petrophysical parameters derived from the wireline log and seismic data provide sub-surface rock and fluid information (Maity and Aminzadeh, 2012; Saadu and Nwankwo, 2018; Mondal et al., 2021). The log data are acquired in the depth domain whereas seismic data are recorded in the time domain. Both the domain has some advantages and limitations. Well log data have higher resolution and provides less areal coverage whereas seismic data provides a much lower resolution with a greater areal extent. Therefore, combining well log and seismic data gives a finer description of reservoir properties on a wider scale (Hampson et al., 2001; Mondal et al., 2020). The seismic section provides structural information about the fault and bedding plane but, the prime input for quantitative interpretation of subsurface formation is obtained from well log analysis and seismic inversion. Numerous seismic inversion methods are used such as maximum likelihood inversion, approximation computation, spars spike, band-limited impedance, Bayesian regularization, and model-based inversion (Hampson and Russell, 1985; Sacchi and Ulrych, 1996). Among these methods, model-based inversion is widely used because it estimates the absolute acoustic impedance with greater correlation and maps the low-frequency content beyond the seismic band by using a bandpass filter (Mallick, 1995). Seismic inversion generates attributes by applying the mathematical transform that contains meaningful information and provides a better understanding of the reservoir properties. The geostatistical approach uses a linear relationship for integrating seismic attributes and reservoir parameters but it does not consider a non-linear relationship, whereas the application of neural network (NN) proves effective in dealing with the complex problem by using a non-linear relationship (Saggaf et al., 2003). Amongst numerous NN architectures developed, multi-layered feed-forward neural network (MLFN) and probabilistic neural network (PNN) are discussed in this paper. The MLFN and PNN delineate the reservoir properties such as P-wave velocity (V_P), S-wave velocity (V_S), density, and pore pressure (Shahraeeni and Curtis, 2011). However, the selection of the best model from several mathematical models with the same output remains the most crucial task for geoscientists. In the Raniganj basin, very limited studies are found in the literature related to mapping reservoir properties using seismic inversion and NN architectures with associated challenges. Hence, the main aim of the study includes (i) reservoir characterization from model-based seismic inversion, (ii) mapping of reservoir properties using NN architectures, and (iii) geological and engineering analysis for implications of hydraulic fracturing treatments in reservoir development and, (iv) associated challenges and limitations in resolving of thin coal seams.

GEOLOGICAL SETTING AND DATASETS OF THE STUDY AREA

Raniganj basin is part of peninsular India is mainly located in the state of West Bengal. The basin has an extension of 3000 km^2 containing sediments of lower and upper Gondwana. Structurally the basin is elongated and semi-elliptical in shape along the E-W direction and shows a typical half-graben configuration. The boundary and intrabasinal faults are the major faults in the basin (Ghosh, 2002). The Salma dyke observed trends in NNW-SSE to NW-SE direction is a significant igneous intrusion that divides the basin into two equal parts (Coal Atlas of India, 1993; Chatterjee et al., 2019; Banerjee and Chatterjee, 2022) (Fig.1). The coal seam near the dyke shows injected

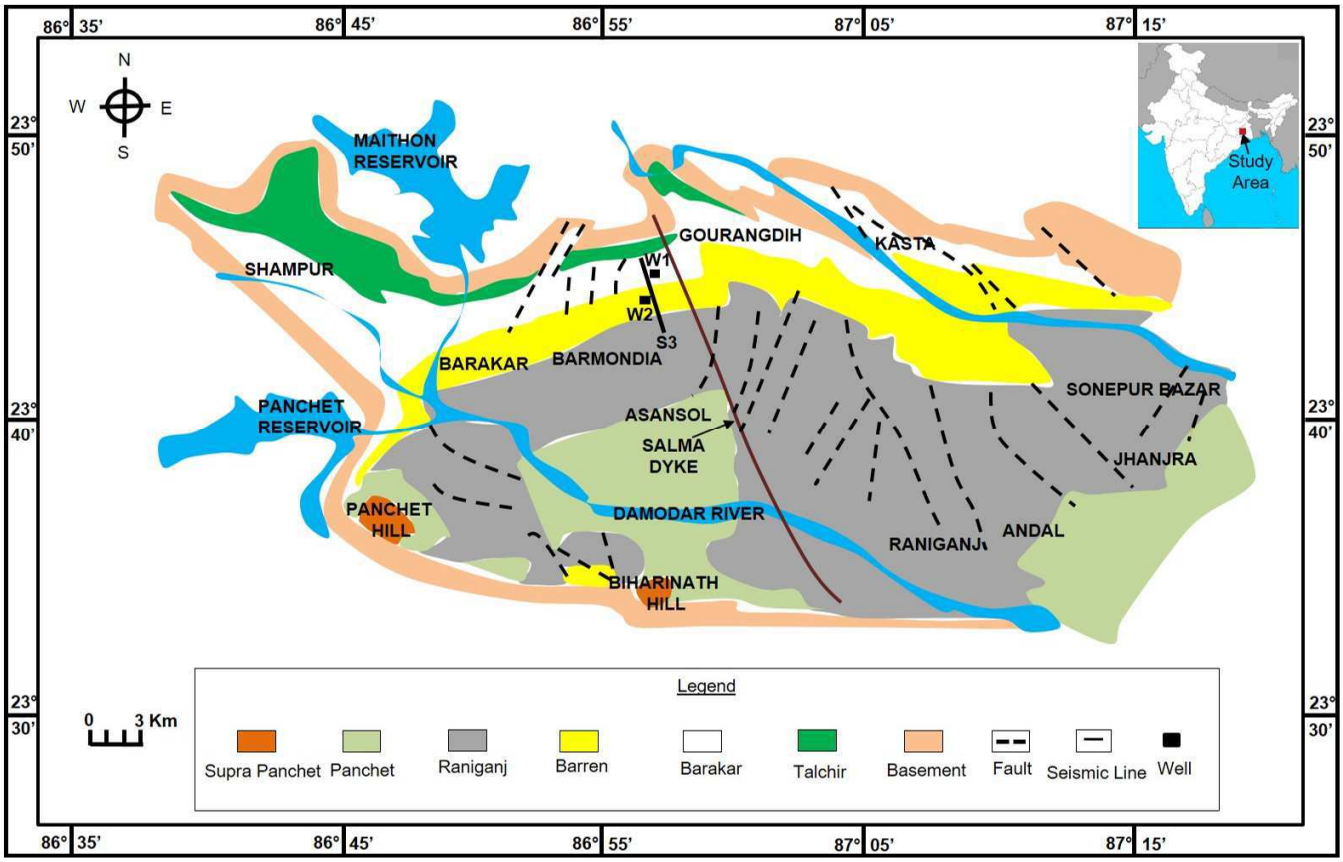

Fig. 1. Geological map of the study area representing the geological formation, seismic line, and well locations. (After Coal Atlas of India, 1993; Banerjee and Chatterjee, 2022).

minerals such as pyrite and siderite in the maceral content, which is due to thermal metamorphism during igneous intrusion (Sarana and Kar, 2011). The formations from the bottom of the reservoir include basement, Talchir, Barakar, Barren measure, Raniganj, Panchet, and Supra-Panchet (Banerjee and Chatterjee, 2021a). The Raniganj basin hosts commercial coal deposits in both Barakar and Raniganj formations. The study area contains wells named W1 and W2, and only one 2D post-stack time migration seismic section (S3) along the NW-SE direction is available. In both wells, geophysical logs- gamma-ray (GR), resistivity (RES), P-wave slowness (DTC), and density (DEN) are recorded, while neutron (NEU) has been recorded well W2. In another nearby well, S-wave slowness (DTS) is available. The coal seams are distinguished from other lithology based on cut-off criteria from geophysical well logs, tabulated in Table 1.

METHODS

The 2D seismic data acquired in the Raniganj basin is intensively covered with coal mines activities, thickly populated townships, villages, and other logistics. The data was acquired in symmetrical split spread geometry with shot interval 10m, receiver interval 5m with 300 receivers on both sides of the shot was designed for higher foldage of 150 and closer spatial sampling. The data was recorded for 6 seconds in a high-frequency spectrum of 1 ms sampling interval. The recorded data quality in the entire area is significantly affected by the presence of cultural noise, that has been generated from man-made activities such as automobile, electric lines, industrial activities, steel pipelines, trains, and highways. The methodology presented in figure 2 illustrates the estimation of reservoir parameters such as shale volume, Young's modulus, and Poisson's ratio from well log and seismic data by implementing model-based post-stack seismic inversion and NN architecture. Also, the detailed steps followed in model-based post-stack seismic inversion are shown in the flowchart. The steps in the flowchart are described in the sub-sections.

Table 1. The distinction of lithology based on cut-off criteria based on well logs parameters.

Lithology	GR (API)	RES (Ohm-m)	DEN (g/cc)	NEU (v/v)
Coal	20-40	500-5000	1.4-1.8	0.50-0.70
Sandstone	55-65	45-70	2.5-2.6	0.08-0.1
Shale	115-160	25-30	2.55-2.6	0.32-0.33
Igneous intrusive	100-200	5-15	2.6-2.8	0.13-0.22

Parameters Estimation

The shale volume (V_{sh}) is determined from the GR log based on equation (Bateman, 1985):

$$V_{sh} = (GR_{\log} - GR_{\min}) / GR_{\max} - GR_{\min}), \quad (1)$$

where $GR_{\log}$, $GR_{\min}$, and $GR_{\max}$ are gamma-ray log magnitude in the formation (API units), clean sand, and shale. Young's modulus is defined from the ratio of linear stress by strain and the ratio of transverse to axial strain determines Poisson's ratio. In an isotropic homogeneous medium, dynamic Young's modulus (E) and Poisson's ratio (PR) in rocks is mathematically expressed as (Boonen, 2003):

$$E = \frac{\rho V_s^2 (3V_p^2 - 4V_s^2)}{V_p^2 - V_s^2} \quad (2)$$

$$PR = \frac{(V_p / V_s) - 2}{2*(V_p - V_s)^2 - 2} \quad (3)$$

where ρ represents the density of the formation. The limitations

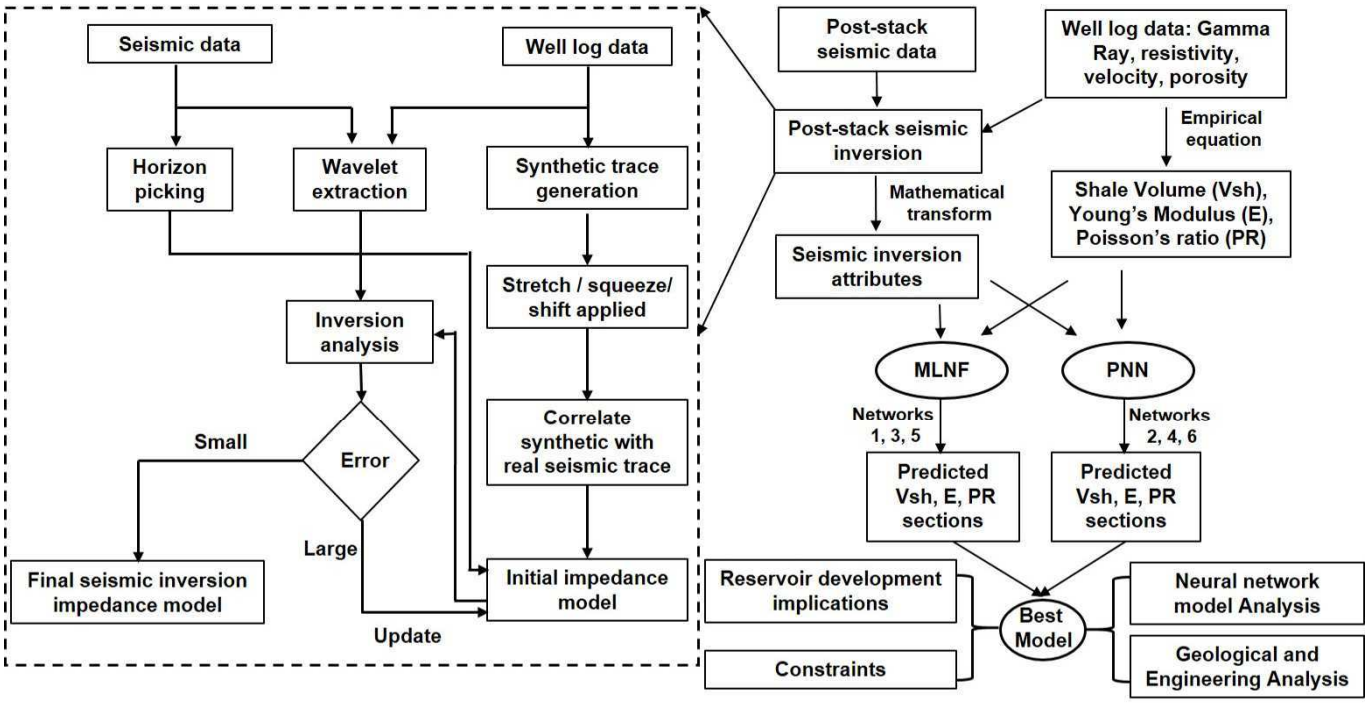

Fig. 2. Flowchart of the study.

of V_s log are a constraint in obtaining dynamic relationships. Therefore, based on available data in a nearby well, a linear relationship between Vp (Km/s) and Vs (Km/s) is obtained with 0.84 as a fitting coefficient (R^2) (Fig. 3). The relationship between Vp and Vs is as follows:

$$V_s = 0.587 * V_p - 0.0869, \quad (4)$$

Model-based Seismic Inversion

Seismic inversion is a mathematical operation of converting reflected acoustic signal in the form of seismic trace, amplitude, and phase into the rock properties such as acoustic impedance (AI), velocity, and density. The transformation of seismic trace into earth reflectivity series is known as deconvolution (Austin et al., 2018). Horizon separates rock layers with different depositional formations and reflection properties. The estimation of AI from the product of density and velocity provides details of reservoir characterization and model-based inversion technique compensates the loss of a low range of frequency components from the seismic data by creating an initial model applying a bandpass filter (Alabi and Enikanselu, 2019). The standard procedure in model-based inversion includes (i) wavelet estimation, (ii) seismic-to-well tie, (iii) horizon picking, (iv) initial model generation, (v) post-stack inversion analysis, and (vi) model-based inversion (Lavergne and Willim, 1977; Hampson et al., 2001). In figure 4a, the seismic section within 150-800 ms represents beds dips (10°-15°) from NW to SE direction, wells position (W1 and W2), picked horizons (H-I, H-II, H-III, H-IV), and few identified faults (dashed lines) (Banerjee and Chatterjee, 2022).

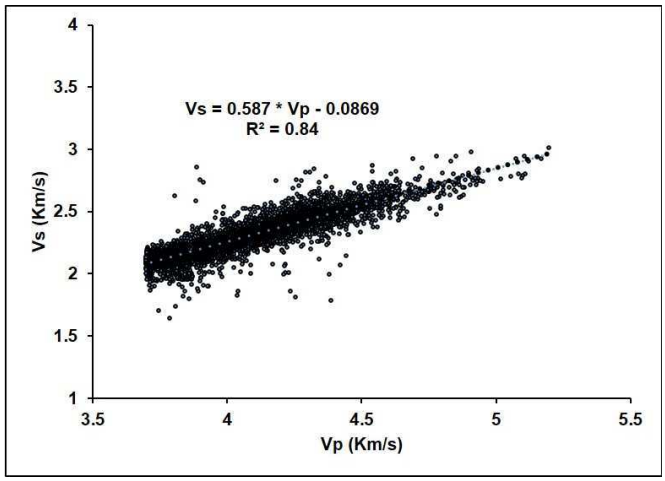

Fig. 3. Cross-plot between Vp (Km/s) versus Vs (Km/s) showing linear relationship.

The acquisition of seismic data in a particular frequency band has missing components of both low and high frequency. The low-frequency components contain useful information about the fluid and porosity in a reservoir which is necessary for obtaining better resolution during the inversion process. The impedance estimation of the initial model is absolute and sensitive to low-frequency components. Therefore, the use of a high-cut filter 10/15 Hz fills the missing frequency in the process of building an initial low-frequency AI model and interpolates along the horizon between the wells. In figure 5, the wavelet time and frequency response are compared between the seismic and the inverted data in the zone of interest from horizon H1 to H4. Figures 5a and 5b illustrate the amplitude spectrum in the time and frequency axis. The frequency of seismic data ranges from 20-120 Hz, while the inverted spectrum in figures 5c and 5d shows the improvement in the frequency range containing dominant frequency below 10 Hz due to the application of a high-cut filter. The minimum misfit between the inverted synthetic and original log is necessary to optimize the inversion parameter of the seismic model at well locations. The best fit parameter gives a higher correlation between the inverted synthetic and original log data (Banerjee and Chatterjee, 2022). The inversion analysis provides the final and best fit from the range of test parameters before initiating the inversion process in the seismic volume. In figures, 4b and 4c, the comparison between synthetic traces (red color) obtained from the inversion result with the input seismic trace (black color), shows the correlation coefficient of 0.99 and 0.97 and measured error of 0.13 and 0.24 in well W1 and W2, respectively. Seismic attributes are the mathematical transformation of seismic trace

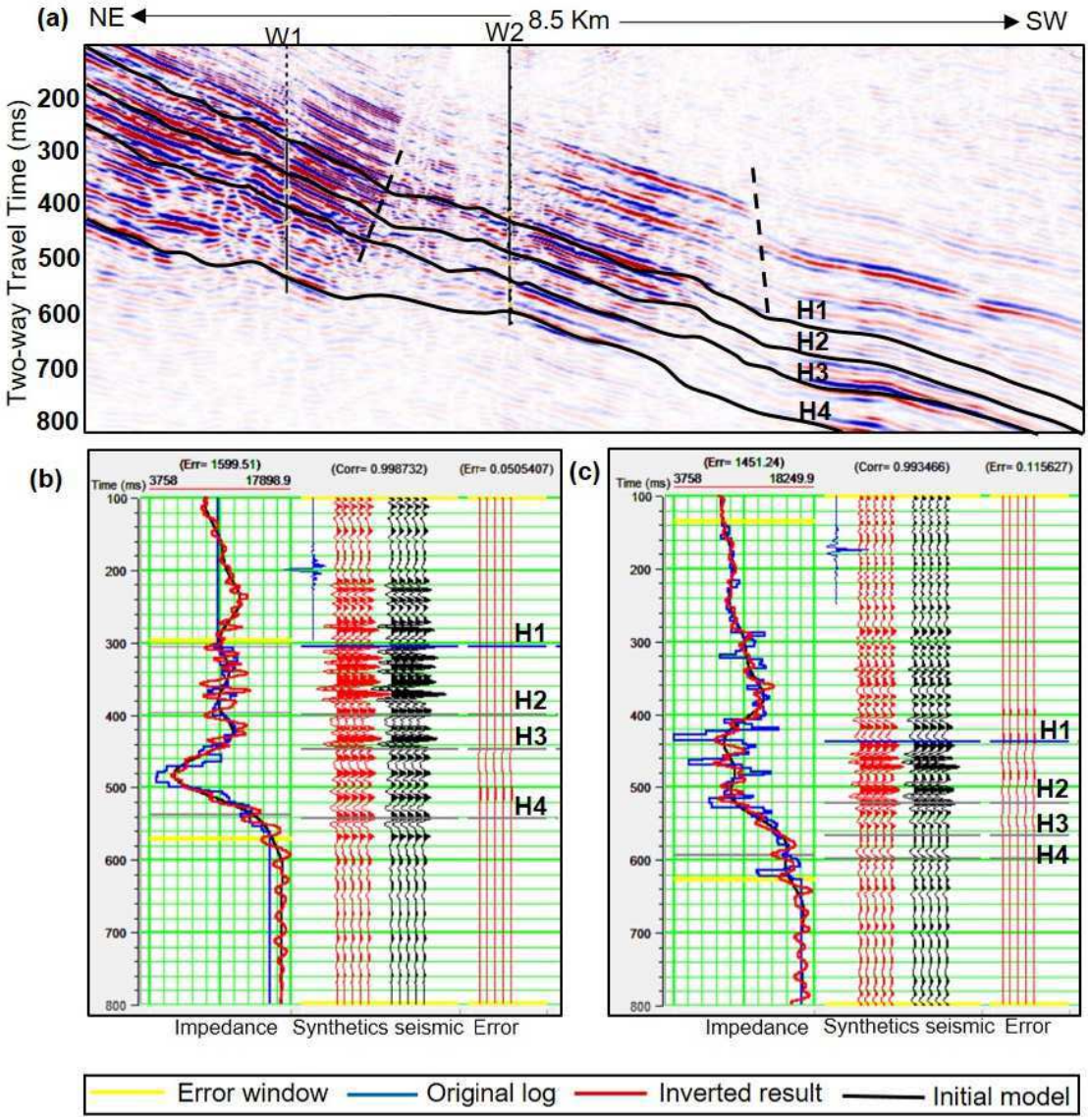

Fig. 4. (a) 2D post-stack time migration seismic section within TWT 150-800 ms representing wells (W1 and W2), picked horizons (H1, H2, H3, H4), and faults (dashed lines), (b) post-stack inversion analysis of well W1 and, (c) post-stack inversion analysis of well W2, representing the original log, inverted results, initial, model, and analysis window (Banerjee and Chatterjee, 2022).

data. In this study, seismic attributes derived from post-stack inversion results, and petro-physical attributes obtained from well log data are used simultaneously. Subsequently, the seismic inversion attributes are integrated with petrophysical attributes to generate linear multivariate regression followed by non-linear neural network methodology. The NN architecture provides better cross-correlation with reduced error compared to multivariate regression. Out of numerous seismic attributes generated, only a few contain meaningful information about reservoir properties and are useful in deriving petrophysical parameters by implementing neural networks.

Neural Network Model

The attributes required to obtain NN models are distinguished into target attributes, training attributes, and final attributes. Attributes such as shale volume, Young's modulus, and Poisson's ratio as target attributes, and seismic inversion attributes are used as training attributes. Few examples of training attributes (inverted results) are quadrature trace, absolute amplitude, instantaneous frequency, instantaneous frequency, and many more. Hence, the specific training attributes having maximum cross-correlation, and minimum training and validation error becomes final attributes. The attributes with the minimum difference between training and validation error are considered for the estimation of shale volume, Young's modulus, and Poisson's ratio. The list of the attributes is tabulated in tables 2, 3, 4. In V_{sh}, the first attribute is considered from 6 attributes. In E, the fifth attribute is considered out of 6 attributes whereas, in PR, the first attribute is considered from 5 attributes. Here, the same training data

Table 2. List of target shale volume attributes, final attributes, training, and validation error.

S. No.	Target	Final Attribute	Training Error	Validation Error
1	Shale volume	Quadrature Trace (Inversion results)	0.09	0.11
2		1/(Inversion results)	0.14	0.15
3		Integrated absolute amplitude (Inversion results)	0.14	0.22
4		Time (Inversion results)	0.13	0.25
5		Amplitude Envelope (Inversion results)	0.13	0.20
6		Amplitude Weighted phase (Inversion results)	0.13	0.37

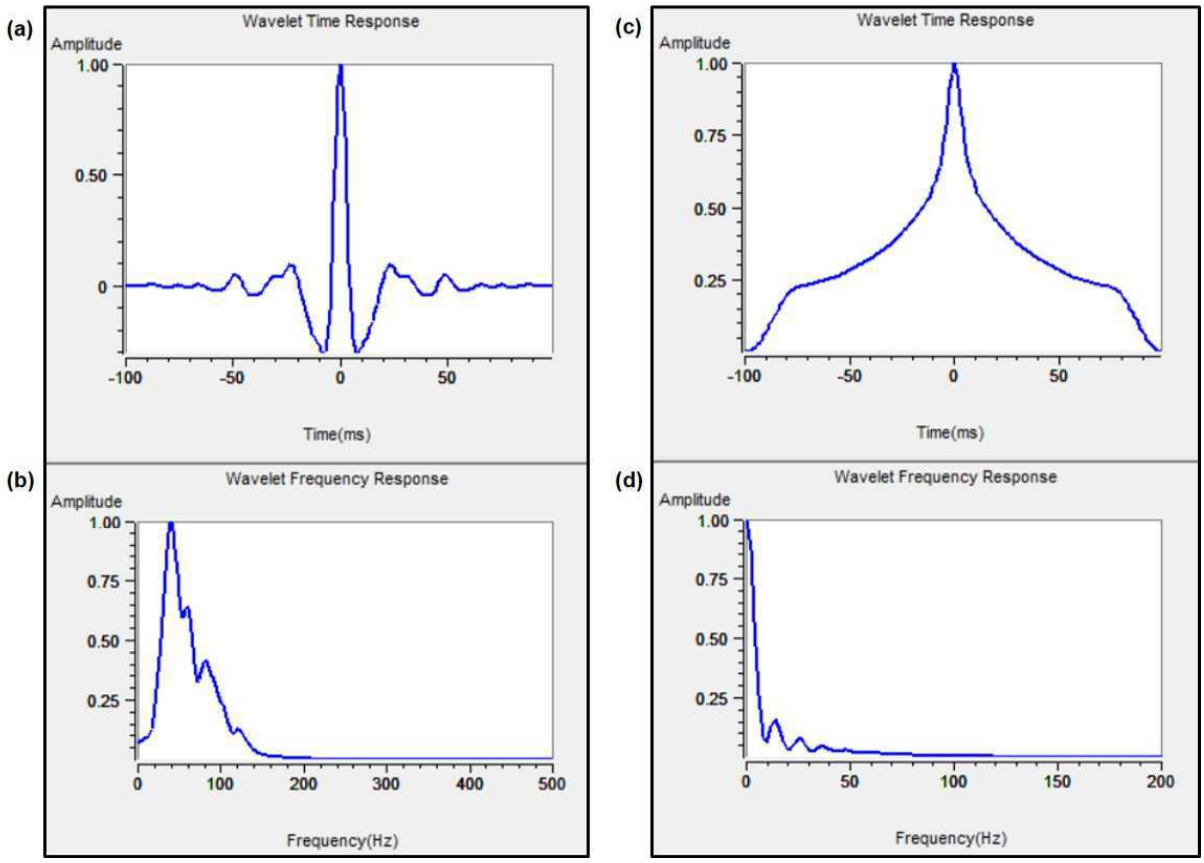

Fig. 5. The wavelet time and frequency response are compared between the seismic and the inverted data in the zone of interest from horizon H1 to H4. **(a)** Amplitude spectrum versus time response of seismic data, **(b)** Amplitude spectrum versus frequency response of seismic data, **(c)** Amplitude spectrum versus time response of inverted seismic data and, **(d)** Amplitude spectrum versus frequency response of inverted seismic data.

and attributes are tested in MLFN and PNN networks keeping W1 as training well and W2 as blind well for validation.

The MLFN model consists of input, hidden, and output layer, where all layer constitutes a particular number of nodes that are connected with weights (Leiphart and Hart, 2001). The training in MLFN from well log data develops optimal weight between nodes, which yields the desired output (Hatampour et al., 2016). The weight is updated using the conjugate gradient optimization technique with a back-propagation procedure, the expression for the calculation of output layer:

$$Y = f\,[\,\alpha_0 + \Sigma_{j=1}^{n_2}\,\alpha_i f_i\,(\,\beta_{0j} + \Sigma_{i=1}^{n_1}\,\beta_{ij} x_i)\,]\,, \qquad (5)$$

Where Y and x are the output and input parameters, á and â act as connecting weights, n_1 and n_2 exhibit the dimension of the input vector and the number of hidden neurons. $\acute{a}_0$ and $\hat{a}_{0j}$ are known as bias weights. The transfer function used in MLFN is a sigmoid function (f) and the common form of the function is (Gogoi and Chatterjee, 2018):

$$sigmoid\,(a) = 1\,/\,(1 + e^{-a}), \qquad (6)$$

Where the value of "a" ranges between 0 and 1. The developed MLFN networks (1, 3, 5) consist of 70 input nodes linking 7 hidden nodes with 150 conjugate-gradient iterations that yield a single output layer. The cross-correlation measures the similarity between actual and predicted results.

The PNN architecture is a mathematical interpolation scheme that replaces the sigmoid transfer function in MLFN with an exponential function (Mohebali et al., 2020). PNN consists of input, pattern, summation, and output layer. The PNN is understood much better than MLFN by examining the mathematical expression in the analysis windows of the training data set consisting of a series of seismic samples and wells, where PNN represents the current output log in a linear combination of the log magnitude in the training data (Hampson et al., 2001). The current log magnitude *L(x)* is formulated as:

Table 3. List of target Young's modulus attributes, final attributes, training, and validation error.

S. No.	Target	Final Attribute	Training Error (GPa)	Validation Error (GPa)
1	Young's modulus	Instantaneous frequency	0.45	0.96
2		Cosine instantaneous phase	0.46	0.98
3		Integrated absolute amplitude	0.47	0.96
4		Derivative instantaneous amplitude	0.48	0.97
5		Derivative (Inversion results)	0.49	0.92
6		Amplitude Weighted frequency	0.50	0.94

Table 4. List of target Poisson's ratio attributes, final attributes, training, and validation error.

S. No.	Target	Final Attribute	Training Error	Validation Error
1	Poisson's ratio	Log (Inverted results)	0.01	0.01
2		Square root (Inverted results)	0.01	0.02
3		1/(Inverted results)	0.01	0.02
4		$(\text{Inverted results})^2$	0.01	0.05
5		(Inverted results)	0.01	0.03

$$L(x) = \frac{\Sigma_{i=1}^{n} L_i \, e^{-(D(x,xi))}}{\Sigma_{i=1}^{n} e^{-(D(x,xi))}} \quad (7)$$

$$\text{where D (x, xi)} = \Sigma_{j=1}^{m} [\, (x_j - x_{ij}) / \sigma_j \,]^2 \quad (8)$$

$D(x, x_i)$ denotes the distance between the input and each training point (x_i) in multi-dimensional space, n is training examples from m attributes, L_i is the measured target log values, σ_j is the smoothing parameter in the training of the network. The prediction error is controlled by the parameters σ_j which is minimized by applying a nonlinear conjugate gradient algorithm (Grana and Della Rossa, 2010). Here, PNN networks (2, 4, 6) are tested with 25 smoothing parameters ranging from 0.1 to 3.0 comprising 100 iterations.

Table 5. Comparison of six networks by implementing NN architectures in the estimation of the volume of shale, Young's modulus, and Poisson's ratio.

Network	Type	Cross-correlation	Training error	Validation error
Estimated volume of shale models				
Network-1	MLFN	0.86	0.09	0.11
Network-2	PNN	0.8	0.1	0.12
Estimated Young's modulus (E) models				
Network-3	MLFN	0.88	0.82 GPa	1.57 GPa
Network-4	PNN	0.96	0.49 GPa	0.92 GPa
Estimated Poisson's ratio (PR) models				
Network-5	MLFN	0.85	0.01	0.01
Network-6	PNN	0.80	0.01	0.01

RESULTS

Neural Networks Model Analysis

The cross-correlation, training, and validation error of MLFN and PNN networks compares the actual and predicted results for shale volume (Figs. 6a and 6b), Young's modulus (Figs. 6c and 6d), and Poisson's ratio (Figs. 6e and 6f) is tabulated in Table 5. Analysis from Table 5 and Fig.5 emphasizes that the MLFN model using networks-1 and 5 gives better results in shale volume and Poisson's ratio estimation (Figs. 6a and 6e) whereas the PNN model using network-4 yields effective Young's modulus output (Fig. 6d). In the best shale volume, Young's modulus, and Poisson's ratio model, cross-correlation are 0.86, 0.96 and 0.85, training error are 0.09, 0.49 GPa and 0.01, validation error are 0.11, 0.92 GPa and 0.01, respectively.

Geological and Engineering Analysis

The AI section distinguishes coal, shale, and sandstone and identifies the top of Barakar and Talchir formations. The relatively thicker coal seam (30-40 m) is better distinguished in the AI section compared to the thinner coal seam (1-10 m). In Fig.7a, the color codes show AI ranges from 5000 to 16,000 (g/cc)*(m/s) in the reservoir. In shale, AI varies from 10000-16000 (g/cc)*(m/s), mix of sandstone and shale, it ranges from 5500-10000 (g/cc)*(m/s), and in coal, AI ranges from 5000-6000 (g/cc)*(m/s) (Banerjee and Chatterjee, 2022). The green color represents coal and the red/blue color represents lithology with higher shale content, while the yellow represents the mix of shale and sand. The best-mapped sections within 150-800 ms are represented in Figs. 7b, 7c, and 7d, respectively. The section in figure 7b shows the shale volume distribution from 15% to 55%. In coal, shale, and sandstone the distribution of shale volume are 15-20%, 30-35%, and 15-30% respectively. In Fig.7c, Young's modulus ranges from 0.5 to 9.5 GPa, and it varies from 0.5-2.5 GPa, 6.5-9.5 GPa, and 4.0-6.0 GPa in coal, shale, and sandstone. In Fig.7d, the Poisson's ratio ranges from 0.23 to 0.27, wherein coal, shale, and sandstone vary from 0.26-0.27, 0.23-0.25, and 0.24-0.26. The Young's modulus versus Poisson's ratio cross-plot in Fig.8 classifies the coal, shale, and mix of sandstone and shale formations encircled based on brittle and ductile behavior. Figure 8 illustrates the linear increase in brittleness with the increase in depth, as Young's modulus increases and Poisson's ratio decreases. The low Poison's ratio (0.23-0.24) and high Young's modulus (6.5-9.5 GPa) are brittle formations, that are relatively hard and rigid, which is seen in the shale formation whereas formations with a high Poisson's ratio (0.26-0.27) and low Young's modulus (0.5-2.5 GPa) are ductile with soft characteristics, which is observed in coal. The intermediate-range of Poisson's ratio (0.24-0.26) and Young's modulus (4.0-6.0 GPa) are formations containing a mix of sandstone and shale.

DISCUSSION

The geological model is always been the starting point for prospect identification, reservoir characterization, or geomechanical modeling.

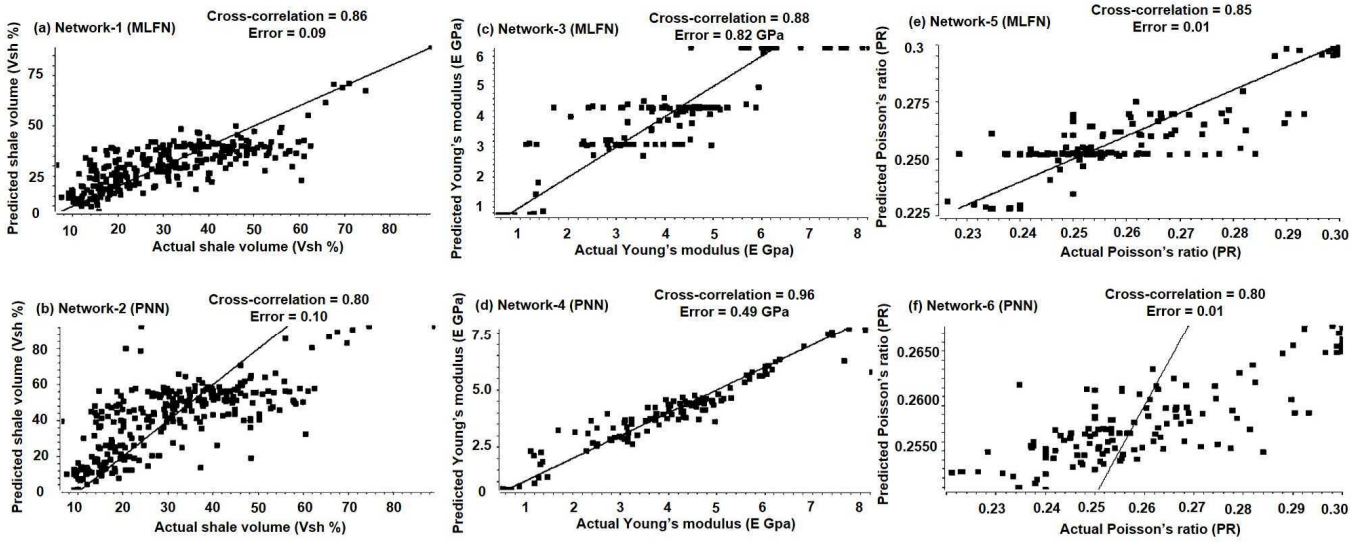

Fig. 6. Cross-correlation between (i) actual and predicted shale volume (V_{sh}) mapping using **(a)** network-1 (MLFN) **(b)** network-2 (PNN); (ii) actual and predicted Young's modulus (E) mapping using **(c)** network-3 (MLFN) **(d)** network-4 (PNN) and; (iii) actual and predicted Poisson's ratio (PR) mapping using **(e)** network-5 (MLFN) **(f)** network-6 (PNN).

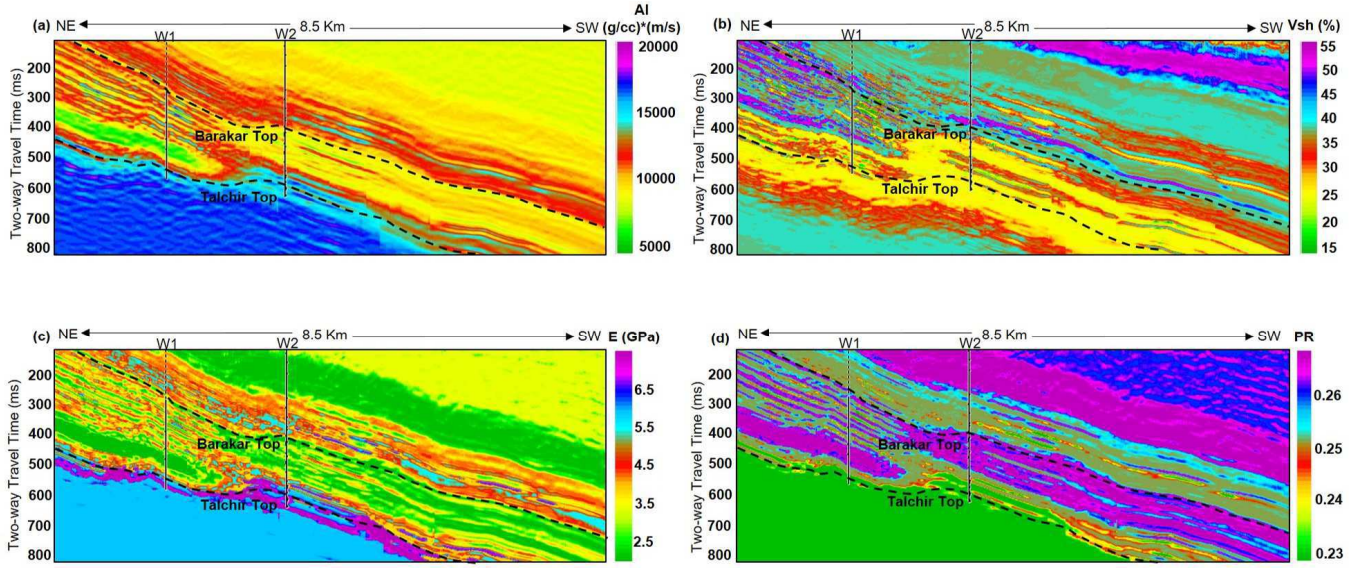

Fig. 7. (a) Post-stack acoustic impedance (AI) inversion section representing AI magnitude ranging from 5000 to 16,000 (g/cc)*(m/s) (Banerjee and Chatterjee, 2022). **(b)** Shale volume (V_{sh}) distribution of MLFN model from 15-55 % in a reservoir. **(c)** Young's modulus (E) distribution of PNN model from 0.3-20 GPa in a reservoir. **(d)** Poisson's ratio (PR) distribution of MLFN model from 0.23-0.27 in a reservoir

Young's modulus and Poisson's ratio are the significant input parameters in designing hydraulic fracturing simulation models in coal seam (Tan et al., 2019). The presence of higher shale volume in overlying and underlying coal seams acts as a good shale barrier due to its higher compressive strength and lower permeability for restricting the hydraulic fracturing fluid movement beyond the coal seam. High stiffness in the shale can withstands higher stress during hydraulic fracturing fluid injection. Thus, the demarcation of the shale layers provides information about continuity and extension. Young's modulus is associated with matrix shrinkage that affects the porosity, permeability, gas recovery rate, and in-situ stress condition of the coalbed methane reservoir (Chatterjee et al., 2019; Banerjee and Chatterjee 2021b). The seismic resolution depends on the wavelength, velocity, and frequency of seismic waves in the formation. The higher impedance contrast in coal distinguishes coal from other formations. However, the thinner coal seams are not effectively distinguishable in the section as the lower acoustic impedance of coal leads to higher reflectivity of acoustic waves from beds and lesser transmissivity to the sub-surface layer; and Rayleigh's limiting criteria for vertical resolution, where bed thickness is less than one-fourth the dominant wavelength cannot be resolved, hence bed thickness less than 10.0 m is not resolved. Moreover, the presence of cultural noise significantly affects the data quality.

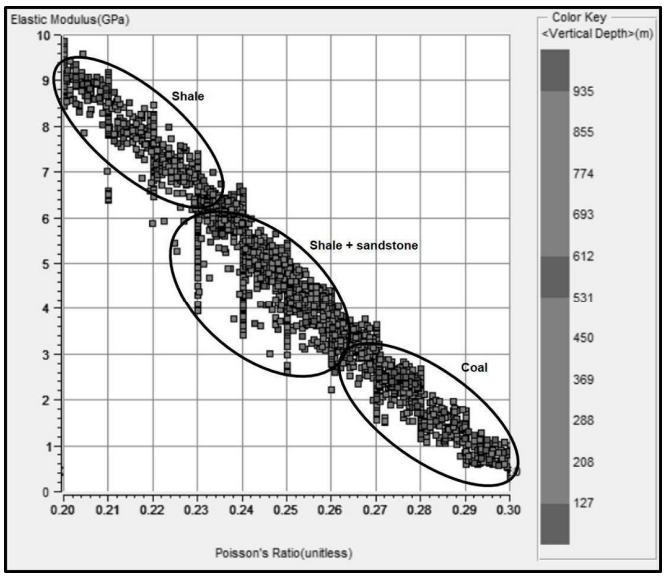

Fig. 8. Poisson's ratio Vs. Young's modulus's cross-plot in the reservoir. The encircled lithology of coal, shale and a mix of shale and sandstone is shown.

CONCLUSIONS

The following conclusion from the study are:

(1) Reservoir characterization using a model-based seismic inversion technique is attempted in the basin having data constraints. Based on acoustic impedance contrast the lithology is distinguishable in the reservoir, however, limitation exists in resolving thin coal seams that mainly depends on the frequency of seismic wave controlled by the geological factors. The use of seismic inversion attributes is vital in estimating reservoir properties and development planning for drilling successful wells and effective reservoir management.

(2) The application of non-linear relationships in the neural network provides effective results with minimum error. The best result selection depends on the cross-correlation between observed and predicted parameters of either MLFN or PNN models. The quantitative estimation of properties like modulus, brittleness will provide crucial input for designing the hydro-fracturing job in the future for optimizing the gas production from this reservoir. Moreover, the derived reservoir properties from this study will help in further geomechanical analysis.

Acknowledgments: The authors are thankful to Oil and Natural Gas Corporation Limited, India for providing data, and supporting us to conduct the research work. The authors are also grateful to Mr. A. K Dwivedi, Ex-Director (Exploration), ONGC, Mr. N. C. Pandey, Ex-Director (T&FS), ONGC, Mr. Aditya Johri (Asset Manager) ONGC Bokaro and Prof. Rajiv Shekhar (Director, IIT-ISM, Dhanbad, India) for the support and encouragement for the research work. Authors acknowledge financial support from SERB/IMP/2018/000369 project.

References

Alabi, A. and Enikanselu, A.P. (2019) Integrating seismic acoustic impedance

inversion and attributes for reservoir analysis over 'DJ' field, Niger Delta. Jour. Petrol. Explor. Prod. Tech., v.9, pp.2487–2496. doi:10.1007/s13202-019-0720-z

Austin, O., Onyekuru, S.O., Ebuka, O.A. and Abdulrazzaq, T.Z. (2018) Application of model-based inversion technique in a field in the coastal swamp depo belt, Niger delta. Internat. Jour. Advan. Geosci., v.6(1), pp.122-126.

Banerjee, A., and Chatterjee, R. (2021a) A Methodology to Estimate Proximate and Gas Content Saturation with Lithological Classification in Coalbed Methane Reservoir, Bokaro Field, India. Natural Resour. Res., v.30, pp.2413-2429. doi:10.1007/s11053-021-09828-2.

Banerjee, A., and Chatterjee, R. (2021b) Fracture analysis using Stoneley wave in coalbed methane reservoir. Near Surface Geophysics. doi:10.1002/nsg.12176.

Banerjee, A., and Chatterjee, R. (2022) Pore pressure modeling and in situ stress determination in Raniganj basin, India. Bull. Engg. Geol. Environ., v.81, 49. doi:10.1007/s10064-021-02502-0

Bateman, R.M. (1985) Openhole Log Analysis and Formation Evaluation. Pretice Hall PTR, New Jersey, 647p.

Boonen, P. (2003) Advantages and challenges of using logging-while-drilling data in rock mechanical log analysis and wellbore stability modeling. *In*: Proceedings AADE National Technology Conference, Texas; 1–3 April 2003.

Chatterjee, R., Paul, S., and Pal, P.K. (2019) Relation between coalbed permeability and in-situ stress magnitude for coalbed methane exploration in Jharia and Raniganj coalfields, India. The Leading Edge, pp.800-807. https://doi.org/10.1190/tle38100800.1

Coal Atlas of India (1993) Central Mine Planning and Design Institute Ranchi. Coal India.

Ghosh, S.C. (2002) The Raniganj Coal Basin: an example of an Indian Gondwana rift. Sediment. Geol., v.147, pp.155-176. doi: 10.1016/S0037-0738(01)00195-6

Grana, D. and Della Rossa, E. (2010) Probabilistic petrophysical properties estimation integrating statistical rock physics with seismic inversion. Geophysics, v.75, pp.O21-O37. doi:10.1190/1.3386676

Gogoi, T. and Chatterjee, R. (2018) Estimation of petro-physical parameters using seismic inversion and neural network modeling in Upper Assam basin, India. Geoscience Frontiers, v.10, pp.1113-1124. doi:10.1016/j.gsf.2018.07.002

Hampson, D. and Russell, B. (1985) Maximum-likelihood seismic inversion. Geophysics, v.50(8), pp.1380-1381.

Hampson, D., Schuelke, J. and Quirein, J. (2001) Use of multi-attribute transforms to predict log properties from seismic data. Geophysics, v.66, pp.220-236.

Hatampour, A., Schaffie, M. and Jafari, S. (2016) Estimation of NMR total and free fluid porosity from seismic attributes using intelligent systems: a case study from an Iranian carbonate gas reservoir. Arabian Jour. Sci. Engg., v.42, pp.315-326.

Lavergne, M., and Willim, C. (1997) Inversion of seismogram and pseudo velocity logs. Geophys. Prospect., v.25, pp.231-250. doi:10.1111/j.1365-2478.1977.tb01165.x

Leiphart, D., and Hart, B.S. (2001). Comparison of linear regression and a probabilistic neural network to predict porosity from 3-d seismic attributes in lower brushy canyon channeled sandstones, Southeast New Mexico. Geophysics, v.66, pp.1349-1358.

Maity, D., and Aminzadeh, F. (2012) Reservoir characterization of an unconventional reservoir by integrating micro-seismic, seismic, and well log data. *In*: SPE western regional meeting, 21-23 March, 2012, Bakersfield, California, USA: Society of Petroleum Engineers. doi:10.2118/154339-MS

Mallick, S. (1995) Model-based inversion of amplitude-variations-with-offset data using a genetic algorithm. Geophysics, v.60(4), pp.939-954.

Mondal, S., Yadav, Y., and Chatterjee, R. (2020) Rock physics forward modeling to predict seismic behavior: A case study for exploration target in Mahanadi basin, east coast of India. Geophys. Prospect., v.68, pp.2186-2194. doi:10.1111/1365-2478.12983.

Mohebali, B., Tahmassebi, A., Mayer-Baese, A. and Gandomi, A.K. (2020) Probabilistic neural networks: a brief overview of theory, implementation, and application. Handbook of Probabilistic Models, pp.347-367. doi:10.1016/B978-0-12-816514-0.00014-X.

Mondal, S., Chatterjee, R. and Chakraborty, S. (2021). An integrated approach for reservoir characterization in deep-water Krishna-Godavari basin, India: A Case study. Jour. Geophys. Engg., v.18, pp.134-144.

Saadu, Y.K. and Nwankwo, C.N. (2018) Petrophysical evaluation and volumetric estimation within Central swamp depobelt, Niger Delta, using 3-D seismic and well logs. Egyptian Jour. Petrol., v.27, pp.531-539. doi:10.1016/j.ejpe.2017.08.004

Sacchi, M.D. and Ulrych, T.J. (1996) Bayesian regularization of some seismic operators. Maximum entropy and Bayesian methods. *In:* Hanson, K.M. and Silver, R.N. (Eds.), Kluwer Academic Publishers, v.79, pp.425-436.

Saggaf, M.M., Toksoz, M.N. and Mustafa, H.M. (2003) Estimation of Reservoir Properties from Seismic Data by Smooth Neural Networks. Geophysics, v.68, pp.1969-1983. doi:10.1190/1.1635051

Sarana, S. and Kar, R. (2011) Effect of igneous intrusive on coal microconstituents: Study from an Indian Gondwana coalfield. Internat. Jour. Coal Geol., v.85(1), pp.161-167

Shahraeeni, M.S. and Curtis, A. (2011) Fast probabilistic non-linear petrophysical inversion. Geophysics, v.76, pp.E45-E58.

Tan, P., Jin, Y., Yuan, L. et al., (2019) Understanding hydraulic fracture propagation behaviour in tight sandstone-coal interbedded formations: an experimental investigation. Petroleum Sci., v.16, pp.148-160. doi:10.1007/s12182-018-0297-z.